

# Faithful Label-free Knowledge Distillation

Evelyn J. Mannix  
Melbourne Centre for Data Science  
University of Melbourne  
Melbourne, Australia 3010  
evelyn.mannix@unimelb.edu.au

Liam Hodgkinson  
University of Melbourne  
Melbourne, Australia 3010  
lhodgkinson@unimelb.edu.au

Howard Bondell  
Melbourne Centre for Data Science  
University of Melbourne  
Melbourne, Australia 3010  
howard.bondell@unimelb.edu.au

## Abstract

Knowledge distillation approaches are model compression techniques, with the goal of training a highly performant student model by using a teacher network that is larger or contains a different inductive bias. These approaches are particularly useful when applied to large computer vision foundation models, which can be compressed into smaller variants that retain desirable properties such as improved robustness. This paper presents a label-free knowledge distillation approach called *Teacher in the Middle (TinTeM)*, which improves on previous methods by learning an approximately orthogonal mapping from the latent space of the teacher to the student network. This produces a more faithful student, which better replicates the behavior of the teacher network across a range of benchmarks testing model robustness, generalisability and out-of-distribution detection. It is further shown that knowledge distillation with *TinTeM* on task specific datasets leads to more accurate models with greater generalisability and OOD detection performance, and that this technique provides a competitive pathway for training highly performant lightweight models on small datasets. Code is available on [GitHub](#).

## 1. Introduction

Computer vision approaches based on neural networks and deep learning have become the standard approach for automating vision problems across a range of fields, from medical imaging [51] and analysis of satellite imagery [4] to detecting weapons in luggage [1]. However, conventional approaches can have poor robustness [3, 16] and struggle to

detect out-of-distribution (OOD) data [27, 45].

Foundation models in computer vision can have superior performance in these challenging circumstances [29, 31]. These follow the success of transformer-based foundation models in language, such as BERT [10], and encode images as vectors in latent space, where the distance between vectors describes the semantic similarity of the images. Two approaches have emerged for training these models — self-supervised learning [29] and contrastive language-image pretraining (CLIP) [31]. The CLIP models were among the

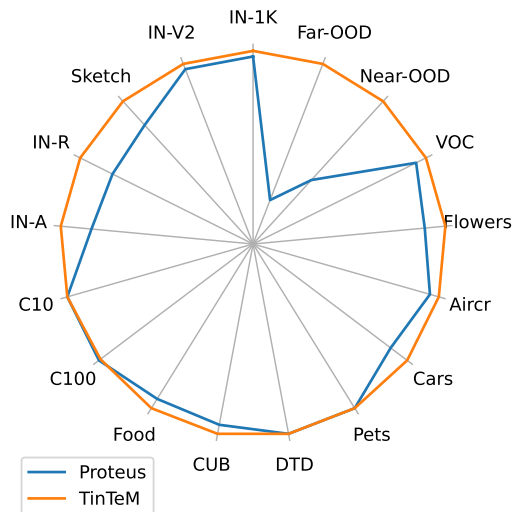


Figure 1. **Effectiveness of knowledge distillation.** Comparison of Proteus and Teacher in the Middle (TinTeM) on a range of benchmarks for distilling knowledge from a DINOv2 ViT-B/14 model into a smaller ViT-S/14 network on ImageNet-1K.

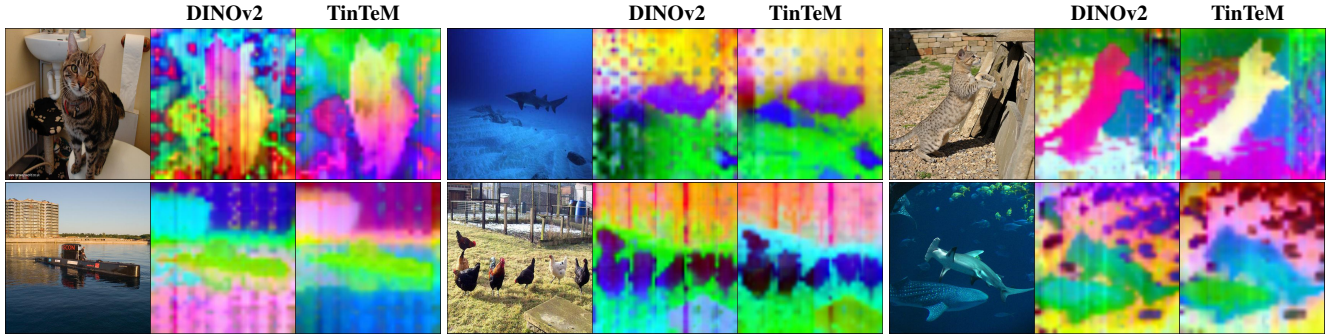


Figure 2. **Patch features.** PCA visualisation of patch features for the DINOv2 ViT-S/14 model, and the distilled ViT-Ti/14 model produced using our Teacher in the Middle (TinTeM) knowledge distillation approach.

first to show that by using a large Vision Transformer (ViT) architecture [11], and a large, diverse and high quality training dataset, a generalist vision model could be produced that obtained high performance across a range of applications [31]. The DINOv2 foundation models followed, and used a combined bootstrapping [8, 14] and masked patch prediction [53] to train foundation models with strong performance on image classification and segmentation tasks [29].

While these foundation models are unnecessarily large for most computer vision applications, knowledge distillation [17] approaches can be used to train smaller models that retain their properties. For instance, the DINOv2 foundation models were distilled from their largest variant by utilising the self-supervised training objective with a larger frozen teacher [29]. This was done on a proprietary dataset and the teacher head weights were never publicly released, preventing this approach from being replicated. A recent knowledge distillation approach, Proteus [52], has shown that it is possible to distill the DINOv2 models and obtain comparable performance on several metrics, without the need for the original dataset. However, sub-optimal results are still obtained for key robustness metrics, generalisability and performance in dense tasks such as image segmentation. Most concerning, however, is that models distilled using Proteus *do not produce faithful reproductions* of the latent space of the teacher model, as shown by their severely reduced performance on OOD detection tasks.

This paper presents Teacher in the Middle (TinTeM), a knowledge distillation approach that learns an explicit mapping between the latent space of the teacher to the student, that preserves distances between points. TinTeM improves the faithfulness of the learned student, *significantly improving OOD detection in comparison to Proteus* (Tab. 1) while achieving competitive performance across all of the considered benchmarks—including classification accuracy, generalisation, robustness and semantic segmentation (Fig. 1). TinTeM reproduces the high-quality patch features of the foundation model (Fig. 2), and can be used to produce spe-

Table 1. **Out-of-distribution detection.** Comparison of performance on the OpenOOD benchmark for the ImageNet-1K dataset. The  $\uparrow$  means larger values are better and the  $\downarrow$  means smaller values are better.

Method	Arch	Teacher	Near OOD		Far OOD	
			AUROC $\uparrow$	FPR $\downarrow$	AUROC $\uparrow$	FPR $\downarrow$
Proteus	ViT-Ti/14	DINOv2 ViT-S/14	64.17	85.73	74.22	67.97
TinTeM	ViT-Ti/14	DINOv2 ViT-S/14	<b>70.49</b>	<b>77.29</b>	<b>91.03</b>	<b>37.21</b>
		DINOv2 ViT-S/14	72.58	74.12	92.67	29.55
Proteus	ViT-S/14	DINOv2 ViT-B/14	61.19	94.56	61.92	86.78
TinTeM	ViT-S/14	DINOv2 ViT-B/14	<b>73.5</b>	<b>73.84</b>	<b>92.93</b>	<b>28.98</b>

cialised models, that have improved accuracy on particular tasks but retain these foundation model properties. In this work, we:

- Present **Teacher in the Middle (TinTeM)**, an approach for distilling Vision Transformer foundation models that learns an approximately orthogonal mapping from the latent space of the teacher to the student, that preserves the distances between images within this latent space.
- Demonstrate that **TinTeM produces a more faithful student model**, that better replicates the performance of the teacher across a range of metrics including robustness, generalisability and out-of-distribution detection.
- Show that **TinTeM can be used to train specialised models** that have improved performance on a particular vision task, but retain foundation model properties such as improved generalisability and out-of-distribution detection performance.

## 2. Related Work

**Knowledge distillation.** Knowledge distillation is the process of transferring knowledge from a large model or model ensemble to a single smaller model. The earliest approaches aligned the output probability vectors of the student and teacher classifications using a Kullback–Leibler (KL) divergence loss [17]. There is a wide range of literature demonstrating how this approach can improve

the performance of smaller Convolutional Neural Networks (CNNs) [42] and Vision Transformers (ViTs) [37, 47], by leveraging a strong teacher or one with different inductive biases to the student model. It has been shown that knowledge distillation is most effective when it is treated as a function matching problem [5], with the same inputs being provided to both the teacher and student model.

Knowledge distillation in the context of a model without class outputs requires an appropriate loss to be crafted such that the student matches the output activations of the teacher, rather than just the class prediction. This is particularly of interest for distilling open-source foundation models, such as the DINOv2 models [29], or for training strong students for object detection and image segmentation. Masked Generative Distillation (MGD) [46] and Proteus [52] undertake knowledge distillation through minimizing the mean squared difference between the student and teacher features, and add an additional masked feature prediction loss analogous to the iBOT self-supervised learning approach [53].

### 3. Methods

**Motivation.** We are interested in the problem of training a student network to mimic the behaviour of a large, high quality teacher model using a ViT architecture, such as the DINOv2 foundation models. A key challenge is that larger ViT architectures have a larger output dimensionality, which prevents the outputs of a smaller student model being directly compared to them.

Proteus [52] addresses this problem by using a student head that maps the outputs of the student network into the latent space of the teacher model, allowing a mean squared error ( $L_2$ ) loss to be applied. However, this approach learns a non-orthogonal linear map into the higher dimensional space, which contains some information on replicating the teacher network and distorts the outputs at the level of the student network which is only indirectly optimised. This reduces the performance of the student, which learns an unfaithful representation of the teacher network that performs particularly poorly at OOD detection.

In theory, one could bypass the requirement of a student head by invoking a Stochastic Neighbour Embedding (SNE) [18, 38] approach, where probability distributions are built to describe the similarity between points in the higher and lower dimensional spaces, so that the difference between them (measured using the KL divergence) can be minimized. Unfortunately, this approach results in a challenging optimization problem that is less efficiently solved by standard gradient-based algorithms in comparison to an  $L_2$  loss.

This paper proposes a more efficient formulation, where a teacher head maps the outputs of the teacher network into the lower dimension space. The teacher head is learned us-

ing an SNE inspired approach that optimizes for orthogonality, allowing a loss to be computed directly with the outputs of the student network in a way that faithfully reproduces the teacher. This is a tractable problem as described by the Johnson–Lindenstrauss (JL) Lemma (Appendix A), which states that such a mapping can be constructed within a certain error that depends on the dimensionality of the target space and the size of the point set [13].

**Notation.** We consider a knowledge distillation setting, where there is a small student network  $S_\theta$  with output dimensionality  $D_S$  and a larger frozen teacher network  $T$  with output dimensionality  $D_T$ . These networks use a ViT architecture, so we assume  $D_T > D_S$ . The loss functions presented in this paper consider a mini-batch stochastic gradient descent setting, defined for a batch of images  $x_i \in \mathbf{X}$ . When only the output class tokens are considered,  $S_\theta^c(x_i), T^c(x_i)$  is used. We write  $S(x_i), T(x_i)$  to refer to a matrix of the concatenated patch token and class token outputs.

**Proteus.** In [52], the authors propose to minimize the mean-squared-error ( $L_2$  loss) between the outputs of the teacher and that of the student, once passed through a dimension-raising map called the student head  $g : \mathbb{R}^{D_S} \rightarrow \mathbb{R}^{D_T}$ . To achieve best performance, they use three student heads with different weights  $\phi, \psi, \nu$  and minimize the  $L_2$  loss separately on the class tokens, features (class and patch tokens), and on randomly masked tokens  $\mathbf{X}^M$  similar to the MGD [46] approach. This leads to the following optimization loss

$$\begin{aligned} \mathcal{L}_{\text{proteus}}(\mathbf{X}; \phi, \psi, \nu, \theta) = & L_2(g_\phi(S_\theta(\mathbf{X})), T(\mathbf{X})) \quad (1) \\ & + L_2(g_\psi(S_\theta^c(\mathbf{X})), T^c(\mathbf{X})) \\ & + L_2(g_\nu(S_\theta(\mathbf{X}^M)^M), T(\mathbf{X}^M)^M) \end{aligned}$$

**TinTeM.** Our approach, Teacher in the Middle (TinTeM), separates the challenge of knowledge distillation into two parts,

$$\mathcal{L}_{\text{TinTeM}}(\mathbf{X}; \phi, \theta) = \mathcal{L}_{\text{dim-red}}(\mathbf{X}; \phi) + \mathcal{L}_{\text{student}}(\mathbf{X}; \theta) \quad (2)$$

Firstly, a teacher head  $h_\phi : \mathbb{R}^{D_T} \rightarrow \mathbb{R}^{D_S}$  is learnt to map the teacher outputs  $T$  to the dimensionality of the student network  $S_\theta$ . This dimensionality reduction loss term  $\mathcal{L}_{\text{dim-red}}$  is independent of fitting the student network. It only requires the target dimension in order to fit the teacher head  $h_\phi$ .

Secondly, the student network  $S_\theta$  is trained to match the image of the teacher under the teacher head  $h_\phi \circ T$  in the student loss term  $\mathcal{L}_{\text{student}}$ . The most effective way to fit this term is to freeze the teacher head  $h_\phi$  gradients and train on both losses concurrently. Using a weighting scheme was observed to produce similar results (Appendix C).

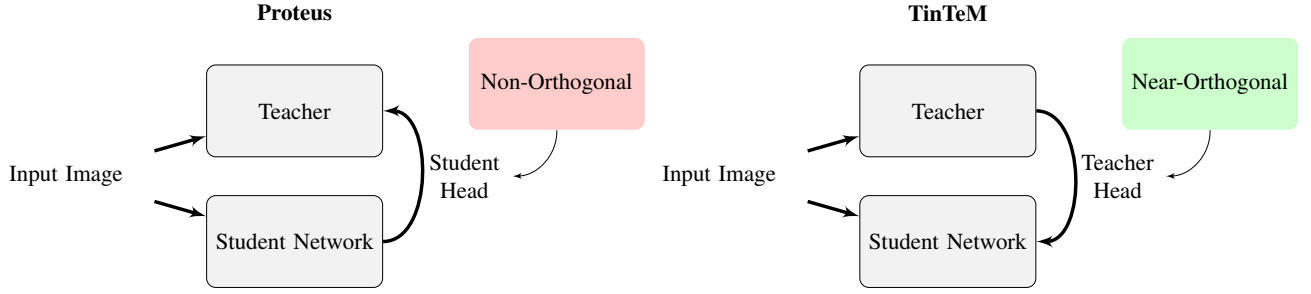


Figure 3. **Knowledge distillation frameworks.** Overview of the Proteus [52] approach (left) and the TinTeM approach (right). In Proteus, student heads  $g$  are used to map the outputs of the student network  $S_\theta$  into the same latent space as the teacher  $T$ , so that a mean squared error ( $L_2$ ) loss can be applied. This leads to a non-orthogonal mapping in the student head, which contains some information helpful to reproducing the teacher outputs. In TinTeM, a teacher head  $h$  is instead used to map the outputs of the teacher  $T$  into a lower dimensional space, allowing the student outputs to be directly compared. The teacher head is trained using a dimensionality reduction loss that learns a near-orthogonal mapping, allowing a more faithful student network to be distilled.

**Dimensionality reduction objective.** The dimensionality reduction objective learns a teacher head  $h_\phi$  that is an orthogonal transformation — a mapping from the outputs of the teacher network that preserves distances between pairs of points in the lower dimensional space  $\mathbb{R}^{D_s}$  of the student. This is considered at two levels — between the image class tokens in a batch, and between the features (patch and class tokens) within an image

$$\mathcal{L}_{\text{dim-red}}(\mathbf{X}; \phi) = L_{\text{KL}}(h_\phi(T^c(\mathbf{X})), T^c(\mathbf{X})) + \frac{1}{|\mathbf{X}|} \sum_i L_{\text{KL}}(h_\phi(T(x_i)), T(x_i)) \quad (3)$$

Within each set of embeddings, an SNE [18, 38] inspired approach can be used where a kernel is defined, and distributions describing the similarity between points are built. The input and output embeddings can then be aligned by minimizing the KL divergence between these distributions.

Cosine similarity provides a natural choice for a distance metric in high dimensions, and is used with foundation models to identify duplicate images [29]. This allows for the von-Mises Fisher distribution to be used as a kernel, where for input vectors  $y$  and  $z$  we have

$$k_\tau(y; z) \propto \exp\left(\frac{y \cdot z}{\|y\| \|z\|} / \tau\right), \quad (4)$$

with temperature  $\tau$  that sets the variance of the distribution. Smaller  $\tau$  values result in a tighter distribution, and larger values are more dispersed.

For a set of vectors in the input space  $p_i \in \mathbf{p}$  and target space  $q_i \in \mathbf{q}$  of size  $N$ , we can define similarity matrices

$P^\tau, Q^\tau$  by

$$P_{ij}^\tau = \frac{p_{j|i} + p_{i|j}}{2N}, \quad p_{j|i} = \frac{k_\tau(p_i; p_j)}{\sum_{i \neq k} k_\tau(p_i; p_k)} \quad (5)$$

$$Q_{ij}^\tau = \frac{q_{j|i} + q_{i|j}}{2N}, \quad q_{j|i} = \frac{k_\tau(q_i; q_j)}{\sum_{i \neq k} k_\tau(q_i; q_k)} \quad (6)$$

where the first equation builds symmetric  $P^\tau, Q^\tau$  matrices, allowing for greater flexibility in the solution. If these  $P^\tau, Q^\tau$  matrices are equal, the cosine similarity between pairs of points in  $\mathbf{p}, \mathbf{q}$  will be equal and  $h_\phi$  will be an orthogonal map. This can be achieved approximately by minimizing the KL divergence ( $D_{\text{KL}}$ ) over a range of temperature values  $\tau$

$$L_{\text{KL}}(\mathbf{p}, \mathbf{q}) = \frac{1}{|\tau|} \sum_{\tau \in \tau} D_{\text{KL}}(P^\tau \| Q^\tau). \quad (7)$$

An ablation study on the best values of  $\tau$  is described in Tab. S20.

**Teacher head architecture.** As done for the Proteus [52] student heads, the teacher head architecture uses a Layer-Norm [2] followed by a linear layer. This can be written as

$$h_\phi(z) = \left( \frac{z - \bar{z}}{\|z\|} \gamma + \beta_1 \right) \mathbf{W} + \beta_2 \quad (8)$$

where  $\bar{z}$  is the average of the  $z$  elements, and the initialization scheme sets the biases  $\beta_1, \beta_2$  to zero and the scaling  $\gamma$  to one at the start of training. The linear map  $W$  is initialized using a random normal distribution as is standard, which is consistent with the mapping constructed in the JL Lemma (Appendix A).

**Student objective.** Similarly to the dimensionality reduction objective, the student loss employs both a class token loss and a feature loss term

$$\mathcal{L}_{\text{student}}(\mathbf{X}; \theta) = L_{\text{cosine}}(S_{\theta}^c(\mathbf{X}), h_{\phi}(T^c(\mathbf{X}))) + L_{\text{cosine}}(S_{\theta}(\mathbf{X}), h_{\phi}(T(\mathbf{X}))) \quad (9)$$

where  $L_{\text{cosine}}$  is based on cosine distance, as given by

$$L_{\text{cosine}}(\mathbf{z}, \mathbf{y}) = \frac{1}{n} \left( \sum_i 1 - \frac{z_i \cdot y_i}{\|z_i\| \|y_i\|} \right) \quad (10)$$

where  $\mathbf{z}, \mathbf{y}$  are sets of input vectors of the same length  $n$ . Considering the teacher head  $h_{\phi}$  learns to conserve cosine similarity, this is also an appropriate metric for the student network and is found to result in better performance than the  $L_2$  loss (Appendix C).

## 4. Experiments: Knowledge distillation

In this section, the TinTeM knowledge distillation approach is compared to Proteus and distilled variants of the DINOv2 models. While we do not have access to the proprietary LVD-142M dataset used to distill the DINOv2 models, it has been shown that ImageNet-1K [33] is sufficient to distill models with comparable accuracy across a range of measures [52].

### 4.1. Experimental setup

Vision Transformer [11] models are distilled using larger DINOv2 teachers on the ImageNet-1K [33] training dataset, comprising 1000 categories across more than 1.2 million images. To enable a fair comparison, we reproduce the results of the Proteus paper and train TinTeM models using a unified codebase. This ensures consistency in the optimizers, samplers, augmentations and other hyperparameters. Following the DINOv2 kNN evaluation [44] and linear probing approach [29] with an additional batchnorm layer [23], evaluations are undertaken on the ImageNet validation set, as well as nine fine-grained classification benchmarks (Oxford Pets [30], FGVC Aircraft [26], Describable Textures [9], Stanford Cars [20], CUB200 [43], CIFAR-10/100 [21], Flowers-102 [28] and Food-101 [7]) and the Pascal VOC 2012 segmentation task [12]. Performance is also tested on several robustness benchmarks including ImageNet-V2 [32], Sketch [40], ImageNet-R [15] and ImageNet-A [16].

We additionally consider the OpenOOD benchmarks [45]. Foundation models are trained on a diverse dataset and excel in this task, and whether distilled students can also perform well has not been previously considered. This section focuses on the ImageNet-1K OpenOOD benchmark, which uses SSB-hard [6] and NINCO [39] as near OOD data, and iNaturalist [19], OpenImage-O [41] and Describable Textures [9] as far OOD data.

Table 2. **ImageNet classification.** Comparison of performance on ImageNet-1K under kNN and linear probing evaluation approaches.

Method	Arch	Teacher	kNN	Linear
Proteus	ViT-Ti/14	DINOv2 ViT-S/14	73.1	76.1
TinTeM	ViT-Ti/14	DINOv2 ViT-S/14	<b>74.3</b>	<b>76.8</b>
		DINOv2 ViT-S/14	79.0	81.1
Proteus	ViT-S/14	DINOv2 ViT-B/14	79.8	82.0
TinTeM	ViT-S/14	DINOv2 ViT-B/14	<b>80.4</b>	<b>82.3</b>

Table 3. **Distillation components.** Results for kNN evaluations on different components of the distillation process for models distilled on ImageNet-1K. For Proteus, results are shown for the class token student head.

Method	Arch	Teacher	kNN			
			Backbone	Student head	Teacher head	Teacher
Proteus	ViT-Ti/14	DINOv2 ViT-S/14	73.1	73.5	78.8	79.0
TinTeM	ViT-Ti/14	DINOv2 ViT-S/14	<b>74.3</b>		78.8	79.0
Proteus	ViT-S/14	DINOv2 ViT-B/14	79.8	80.0		82.1
TinTeM	ViT-S/14	DINOv2 ViT-B/14	<b>80.4</b>		82.1	82.1

Table 4. **Measuring orthogonality.** Frobenius norm of the scaled Gram matrix  $\mathbf{A}/\alpha$  to the identity matrix, using the weight matrices  $\mathbf{W}$  from the teacher and student heads of TinTeM and Proteus. For each matrix  $\alpha$  is set to the mean of the diagonal elements of  $\mathbf{A}$ , which minimises the error.

Method	Arch	Teacher	Gram matrix ( $\mathbf{A}$ )	
			$\mathbf{A} \in \mathbb{R}^{D_T \times D_T}$	$\mathbf{A} \in \mathbb{R}^{D_S \times D_S}$
Proteus	ViT-Ti/14	DINOv2 ViT-S/14	27.3	9.5
TinTeM	ViT-Ti/14	DINOv2 ViT-S/14	<b>20.3</b>	<b>2.6</b>

### 4.2. Results

**TinTeM trains more competitive students.** Tab. 2 shows that TinTeM trains students with better performance in comparison to Proteus [52], for both the linear probing and kNN evaluation methods. It is also found that the teacher head can project the embeddings from the teacher network into the latent space of the student with minimal loss of kNN accuracy, and that the token student head from Proteus has a higher kNN accuracy than the model backbone (Tab. 3). These observations confirm the motivations for TinTeM — the Proteus student heads are not an uninformative mapping into a higher dimensional space, but are contaminated with information relevant for reproducing the teacher model. Further, a high-quality lower dimensional projection from the teacher network is simple to train and provides more effective supervision.

It is also observed in Tab. 2 that the TinTeM and Proteus approaches can outperform the distilled DINOv2 models of the same size. However, it is challenging to determine if these distillation approaches are more effective, as the DI-

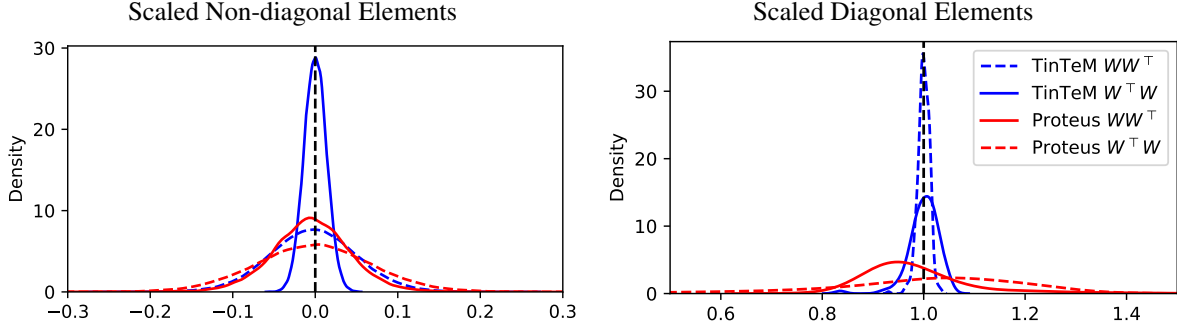


Figure 4. **Visualizing orthogonality.** Kernel density estimate plots of the diagonal and non-diagonal elements for the scaled Gram matrices of the linear maps  $\mathbf{W}$  in the teacher and student heads, drawn from TinTeM and Proteus respectively. A perfectly orthogonal matrix  $\mathbf{W}$  will have a Gram matrix with density on the dashed lines.

Table 5. **Fine-grained classification.** Comparison of performance on fine-grained classification tasks using a linear probe evaluation.

Method	Arch	Teacher	Dataset									
			C10	C100	Food	CUB	DTD	Pets	Cars	Aircr	Flowers	Average
Proteus	ViT-Ti/14	DINOv2 ViT-S/14	<b>95.1</b>	81.4	83.5	84.1	72.9	<b>94.2</b>	72.8	54.1	96.0	81.6
TinTeM	ViT-Ti/14	DINOv2 ViT-S/14	94.9	<b>81.9</b>	<b>84.6</b>	<b>85.1</b>	<b>73.8</b>	94.1	<b>75.3</b>	<b>55.7</b>	<b>96.8</b>	<b>82.5</b>
		DINOv2 ViT-S/14 [29]	97.7	87.5	89.1	88.1	80.6	95.1	81.6	74.0	99.6	88.1
Proteus	ViT-S/14	DINOv2 ViT-B/14	<b>97.8</b>	<b>87.7</b>	89.7	88.4	<b>78.0</b>	<b>95.9</b>	82.8	62.9	97.6	86.8
TinTeM	ViT-S/14	DINOv2 ViT-B/14	<b>97.8</b>	87.6	<b>90.3</b>	<b>88.9</b>	<b>78.0</b>	<b>95.9</b>	<b>84.0</b>	<b>63.4</b>	<b>98.8</b>	<b>87.2</b>

Table 6. **Semantic segmentation.** Comparison of performance on the Pascal VOC 2012 semantic segmentation task using a linear probe.

Method	Arch	Teacher	mIoU
Proteus	ViT-Ti/14	DINOv2 ViT-S/14	70.5
Proteus w/o patch loss	ViT-Ti/14	DINOv2 ViT-S/14	69.7
TinTeM	ViT-Ti/14	DINOv2 ViT-S/14	<b>71.1</b>
		DINOv2 ViT-S/14	81.2
Proteus	ViT-S/14	DINOv2 ViT-B/14	77.3
Proteus w/o patch loss	ViT-S/14	DINOv2 ViT-B/14	77.1
TinTeM	ViT-S/14	DINOv2 ViT-B/14	<b>77.9</b>

Table 7. **Robustness and generalisation.** Comparison of performance on ImageNet-1K robustness and generalisation benchmarks.

Method	Arch	Teacher	Test Dataset			
			IN-V2	Sketch	IN-R	IN-A
Proteus	ViT-Ti/14	DINOv2 ViT-S/14	64.3	25.5	37.8	11.4
TinTeM	ViT-Ti/14	DINOv2 ViT-S/14	<b>64.9</b>	<b>27.9</b>	<b>40.7</b>	<b>13.2</b>
		DINOv2 ViT-S/14 [29]	70.9	41.2	53.7	33.5
Proteus	ViT-S/14	DINOv2 ViT-B/14	72.2	38.4	50.0	29.6
TinTeM	ViT-S/14	DINOv2 ViT-B/14	<b>72.5</b>	<b>40.4</b>	<b>52.3</b>	<b>31.5</b>

NOv2 models were trained on a larger proprietary dataset,

Table 8. **Training time.** Comparison of training time on ImageNet for 300 epochs with a batch size of 1024.

Method	Arch	Teacher	GPUs	Total GPU hours	Total GPU memory
Proteus	ViT-Ti/14	DINOv2 ViT-S/14	1 80GB Nvidia A100	92	55GB
TinTeM	ViT-Ti/14	DINOv2 ViT-S/14	1 80GB Nvidia A100	95	47GB
Proteus	ViT-S/14	DINOv2 ViT-B/14	2 80GB Nvidia A100	182	111GB
TinTeM	ViT-S/14	DINOv2 ViT-B/14	2 80GB Nvidia A100	154	81GB

of which the ImageNet-1K dataset was only a small subset.

**TinTeM learns a scaled orthogonal projection.** It is found that TinTeM learns a linear map  $\mathbf{W}$  in the teacher head (Eq. (8)) that is approximately orthogonal, up to a scaling factor. More concisely, we find that

$$\mathbf{W}^T \mathbf{W} / \alpha \approx \mathbf{I}, \quad \mathbf{W} \mathbf{W}^T / \beta \approx \mathbf{I} \quad (11)$$

where  $\alpha, \beta$  are positive real numbers and  $\mathbf{W}^T \mathbf{W}, \mathbf{W} \mathbf{W}^T$  form Gram matrices. Qualitatively, this can be seen in Fig. 4 where histograms are shown of the elements from Gram matrices formed using the linear map  $\mathbf{W}$  in the TinTeM teacher head and the Proteus class token student head for the ViT-Ti/14 student network. The scaled TinTeM Gram matrices are much closer to the identity matrix, and this is measured quantitatively using the Frobenius norm in Tab. 4.

**TinTeM improves performance on classification tasks.**

Tab. 5 shows that the models distilled by TinTeM have im-

proved or similar performance over Proteus for all downstream fine-grained classification tasks. Competitive accuracy is also achieved with the distilled DINOv2 models of the same size, which TinTeM outperforms on six of the nine datasets. Poorest performance is achieved on the FGVC-Aircraft dataset, which likely reflects differences in the training data used for distillation. The LVD-142M dataset used to train and distill the DINOv2 models contained a million images with high similarity to the FGVC-Aircraft dataset [29], whereas ImageNet only contains a single *airliner* class with approximately 1300 images.

**TinTeM improves segmentation performance.** Tab. 6 shows that TinTeM also improves accuracy on downstream segmentation tasks in comparison to Proteus. TinTeM does not include the masked patch loss objective, that we confirm improves the performance of Proteus on dense tasks, and incorporating it may improve performance further. The DINOv2 distilled model outperforms TinTeM in this case, which reflects that we do not incorporate further pretraining with an increased image resolution and was found to be key to improving the performance of the DINOv2 models on dense tasks [29].

**TinTeM distills a more robust student model.** Tab. 7 shows that TinTeM results in improved performance over Proteus across a range of ImageNet-1K robustness and generalisation benchmarks. The DINOv2 distilled model obtains better performance in this instance for all benchmarks except ImageNet-V2, but TinTeM closes the gap between the ImageNet-1K and LVD-142M distilled models significantly.

**TinTeM reproduces the OOD detection performance of the teacher.** TinTeM is faithful to the teacher networks when it comes to OOD detection performance, as shown in Tab. 1. Proteus performs very poorly on this benchmark, with worse performance observed for higher quality models. In contrast, TinTeM is able to distill models that have strong OOD performance, even outperforming the DINOv2 counterpart.

**TinTeM does not require additional computational resources.** Tab. 8 provides timings and GPU memory usage for fitting the Proteus and TinTeM models described in this section. Training time is similar for the ViT-Ti/14 and DINOv2 ViT-S/14 student-teacher pair, but TinTeM is more efficient for larger models. This is due to the masked patch loss in Proteus, which requires the student network once on unmasked inputs, and a second time on masked inputs. As a result, training is faster for TinTeM for larger students. TinTeM slightly more memory efficient compared to Proteus, and further computational savings could be made by freezing the teacher head  $h_\phi$  once a sufficiently high quality map has been trained.

Table 9. **State-of-the-art lightweight models.** Comparison of best TinTeM models to other approaches for training state-of-the-art lightweight models for specialised tasks.

Method	Arch	Parameters	Dataset			
			C10	C100	Food	Pets
NAT [24]	MobileNetV2 [34]	4.5-9.0M	98.4	88.3	89.4	94.3
CeiT [48]	CeiT-T	6.4M	98.5	88.4		93.8
TinTeM	ViT-Ti/14	5.5M	<b>98.8</b>	<b>89.6</b>	<b>92.7</b>	<b>94.9</b>

## 5. Experiments: Specialist models

This section explores the potential for TinTeM knowledge distillation to improve the performance of specialised models that solve one particular task (e.g. classifying images of food). We refer to this process, where an additional knowledge distillation training step is undertaken on a target dataset, as TinTeM finetuning. This approach can train highly performant small networks, that also have improved results on generalisability and OOD detection benchmarks.

### 5.1. Experimental setup

The TinTeM models distilled in the previous section are compared with models that have been further finetuned with TinTeM — an additional pretraining step where distillation is undertaken on a smaller target dataset of interest. The strong DeiT [37] pretrained weights are also considered, which were trained on ImageNet-1K with a larger CNN network using class-based knowledge distillation.

We focus on a small set of tasks, including CIFAR-10/100 [21], Food-101 [7] and Oxford Pets [30]. Oxford Pets is a challenging dataset for training specialised ViT networks, as it only contains 3680 training images. The CIFAR-10/100 OpenOOD benchmarks [45] and the challenging cartoon subsets of the CIFAR-10-W benchmark [35] are used to test OOD detection and generalisation performance.

The DINOv2 linear probe evaluation method is employed [29], as well as finetuning using the DeiT recipe [37]. When training models with this latter approach, the linear prediction head is trained before finetuning the backbone, to avoid distorting the pretrained features [22].

### 5.2. Results

**TinTeM finetuning improves the performance of specialist models.** Tab. 10 shows that TinTeM finetuning improves downstream performance, even when the training datasets are quite small. For every dataset considered, this additional learning step improves linear probe evaluations with a frozen backbone by a significant margin (1-5%). These benefits remain under the strong DeiT training recipe, which finetunes the model backbone. While CIFAR-10/100 and Food-101 have much stronger results under DeiT finetuning, we find that Oxford Pets has best performance with

Table 10. **Specialist models — accuracy.** Comparison of performance on fine-grained image classification tasks.

Method	Arch	Teacher	Pretraining dataset	Linear				DeiT			
				C10	C100	Food	Pets	C10	C100	Food	Pets
DeiT [37]	ViT-Ti/16	RegNetY-16GF	ImageNet	93.1	77.7	77.7	93.3	98.3	87.8	89.9	<b>93.0</b>
TinTeM	ViT-Ti/14	DINOv2 ViT-S/14	ImageNet	94.9	81.9	84.6	94.1	98.7	89.0	91.7	92.7
TinTeM	ViT-Ti/14	DINOv2 ViT-S/14	ImageNet → Target dataset	<b>97.6</b>	<b>86.3</b>	<b>89.8</b>	<b>94.9</b>	<b>98.8</b>	<b>89.6</b>	<b>92.7</b>	<b>93.0</b>

Table 11. **Specialist models — generalisability.** Comparison of generalisability of specialist models on the cartoon subsets of the CIFAR-10-W benchmark [35]. We report mean per-class accuracy due to dataset imbalances. In-distribution training images (top) and cartoon images (bottom) are included for reference.

Method	Arch	Teacher	Pretraining dataset	Linear				DeiT			
				Diff	Bin	Bai	360	Diff	Bin	Bai	360
DeiT [37]	ViT-Ti/16	RegNetY-16GF	ImageNet	65.9	51.0	47.6	48.8	86.9	62.6	56.0	60.1
TinTeM	ViT-Ti/14	DINOv2 ViT-S/14	ImageNet	70.8	49.5	<b>48.7</b>	<b>50.3</b>	88.5	63.2	56.3	60.7
TinTeM	ViT-Ti/14	DINOv2 ViT-S/14	ImageNet → Target dataset	<b>73.4</b>	<b>52.5</b>	48.6	49.9	<b>89.1</b>	<b>64.1</b>	<b>57.5</b>	<b>61.4</b>

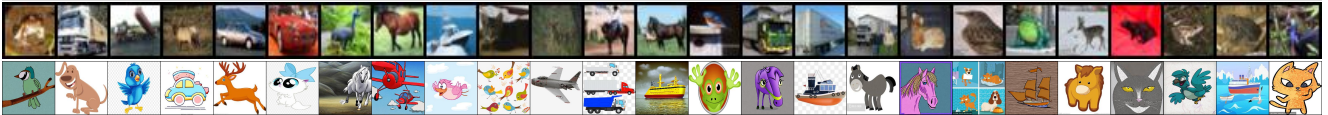


Table 12. **Specialist models — OOD detection.** Comparison of performance on the OpenOOD benchmark [45]. The AUC is reported for detecting OOD images.

Method	Arch	Teacher	Pretraining dataset	Frozen backbone				DeiT finetuned			
				CIFAR-10		CIFAR-100		CIFAR-10		CIFAR-100	
				Near-OOD	Far-OOD	Near-OOD	Far-OOD	Near-OOD	Far-OOD	Near-OOD	Far-OOD
DeiT [37]	ViT-Ti/16	RegNetY-16GF	ImageNet	57.01	47.04	58.14	46.19	96.79	98.69	87.45	86.73
TinTeM	ViT-Ti/14	DINOv2 ViT-S/14	ImageNet	93.44	95.87	85.23	76.37	96.69	98.59	87.90	<b>89.87</b>
TinTeM	ViT-Ti/14	DINOv2 ViT-S/14	ImageNet → Target dataset	<b>95.12</b>	<b>98.02</b>	<b>87.00</b>	<b>80.95</b>	<b>97.05</b>	<b>98.79</b>	<b>89.52</b>	89.53

a linear probe evaluation after TinTeM finetuning. This reflects the small size of the Oxford pets dataset, which makes training ViT networks challenging. Further, Tab. 10 highlights the strong performance of TinTeM finetuning over the pretrained DeiT baseline, with large improvements using a linear probe, and more moderate improvements (excluding Oxford pets) under DeiT finetuning.

A ViT-Tiny network finetuned with TinTeM can have competitive accuracy compared to other approaches in the literature that have been highly optimised to perform well on specialist tasks with a small dataset. Tab. 9 shows that TinTeM finetuning trains competitive networks in comparison to Neural Architecture Search (NAT) [24] and Convolution-enhanced image Transformers (CeiT) [48]. Knowledge distillation approaches like TinTeM are an additional approach, that could be used in conjunction with these techniques to build highly performant specialist vision models.

**TinTeM finetuning improves the generalisability of specialist models.** Tab. 11 shows that TinTeM finetuning

leads to improved generalisability for specialist models on CIFAR-10. Under a linear probing evaluation, TinTeM finetuning strongly improves generalisability on two of the four datasets, and improves generalisability for all datasets even after DeiT finetuning. Tab. 11 further shows consistent generalisability improvements over the baseline DeiT pretrained model.

DeiT finetuning is observed to significantly improve generalisation performance across all initializations, due to extensive use of both mixup [50] and cutmix [49] in the DeiT training recipe.

**TinTeM finetuning improves the OOD detection performance of specialist models.** Tab. 12 shows that TinTeM finetuning leads to improved performance on the OpenOOD [45] benchmark for specialist models on CIFAR-10/100. Without DeiT finetuning, strong improvements in OOD detection are observed under TinTeM finetuning over the ImageNet pretrained baselines. Improvements remain after DeiT finetuning, but are smaller.

DeiT finetuning is also observed to significantly improve



OOD detection across all initializations, which is consistent with prior work showing cutmix [49] to improve performance on these benchmarks.

## 6. Conclusion

This paper introduces TinTeM, a label-free knowledge distillation approach designed to train highly performant student networks from a foundation model teacher with a Vision Transformer [11] architecture. This is achieved by introducing a teacher head, that maps from the higher dimensional latent space of the teacher network into the smaller dimensional space of the student, and training this mapping to preserve the cosine similarity of images within these embedding spaces. TinTeM trains a faithful student, that more closely replicates the behaviour of the teacher network in comparison to the Proteus approach [52], where a student head is used to align the student outputs with the teacher.

## Acknowledgements

We acknowledge the Traditional Owners of the unceded land on which the research detailed in this paper was undertaken: the Wurundjeri Woi-wurrung and Bunurong peoples. This research was undertaken using the LIEF HPC-GPGPU Facility hosted at the University of Melbourne. This Facility was established with the assistance of LIEF Grant LE170100200. This research was also undertaken with the assistance of resources and services from the National Computational Infrastructure (NCI), which is supported by the Australian Government. Evelyn Mannix was supported by a Australian Government Research Training Program Scholarship to complete this work.

## References

- [1] Nikita Andriyanov. Intelligent computer vision systems in the processing of baggage and hand luggage x-ray images. In *Advances in Artificial Intelligence-Empowered Decision Support Systems: Papers in Honour of Professor John Psarras*, pages 283–324. Springer, 2024. 1
- [2] Jimmy Lei Ba. Layer normalization. *arXiv preprint arXiv:1607.06450*, 2016. 4
- [3] Yutong Bai, Jieru Mei, Alan L Yuille, and Cihang Xie. Are transformers more robust than cnns? *Advances in neural information processing systems*, 34:26831–26843, 2021. 1
- [4] Favyen Bastani, Piper Wolters, Ritwik Gupta, Joe Ferdinando, and Aniruddha Kembhavi. Satlaspretrain: A large-scale dataset for remote sensing image understanding. In *Proceedings of the IEEE/CVF International Conference on Computer Vision*, pages 16772–16782, 2023. 1
- [5] Lucas Beyer, Xiaohua Zhai, Amélie Royer, Larisa Markeeva, Rohan Anil, and Alexander Kolesnikov. Knowledge distillation: A good teacher is patient and consistent. In *Proceedings of the IEEE/CVF conference on computer vision and pattern recognition*, pages 10925–10934, 2022. 3
- [6] Julian Bitterwolf, Maximilian Müller, and Matthias Hein. In or out? fixing imagenet out-of-distribution detection evaluation, 2023. 5
- [7] Lukas Bossard, Matthieu Guillaumin, and Luc Van Gool. Food-101—mining discriminative components with random forests. In *Computer Vision—ECCV 2014: 13th European Conference, Zurich, Switzerland, September 6–12, 2014, Proceedings, Part VI 13*, pages 446–461. Springer, 2014. 5, 7
- [8] Mathilde Caron, Hugo Touvron, Ishan Misra, Hervé Jégou, Julien Mairal, Piotr Bojanowski, and Armand Joulin. Emerging properties in self-supervised vision transformers. In *Proceedings of the IEEE/CVF international conference on computer vision*, pages 9650–9660, 2021. 2
- [9] Mircea Cimpoi, Subhransu Maji, Iasonas Kokkinos, Sammy Mohamed, and Andrea Vedaldi. Describing textures in the wild, 2013. 5
- [10] Jacob Devlin. Bert: Pre-training of deep bidirectional transformers for language understanding. *arXiv preprint arXiv:1810.04805*, 2018. 1
- [11] Alexey Dosovitskiy. An image is worth 16x16 words: Transformers for image recognition at scale. *arXiv preprint arXiv:2010.11929*, 2020. 2, 5, 9
- [12] M. Everingham, L. Van Gool, C. K. I. Williams, J. Winn, and A. Zisserman. The PASCAL Visual Object Classes Challenge 2012 (VOC2012) Results. <http://www.pascal-network.org/challenges/VOC/voc2012/workshop/index.html>. 5
- [13] Casper Benjamin Freksen. An introduction to johnson-lindenstrauss transforms. *arXiv preprint arXiv:2103.00564*, 2021. 3, 2
- [14] Jean-Bastien Grill, Florian Strub, Florent Altché, Corentin Tallec, Pierre Richemond, Elena Buchatskaya, Carl Doersch, Bernardo Avila Pires, Zhaohan Guo, Mohammad Gheshlaghi Azar, et al. Bootstrap your own latent—a new approach to self-supervised learning. *Advances in neural information processing systems*, 33:21271–21284, 2020. 2
- [15] Dan Hendrycks, Steven Basart, Norman Mu, Saurav Kadavath, Frank Wang, Evan Dorundo, Rahul Desai, Tyler Zhu, Samyak Parajuli, Mike Guo, et al. The many faces of robustness: A critical analysis of out-of-distribution generalization. In *Proceedings of the IEEE/CVF International Conference on Computer Vision*, pages 8340–8349, 2021. 5
- [16] Dan Hendrycks, Kevin Zhao, Steven Basart, Jacob Steinhardt, and Dawn Song. Natural adversarial examples. In *Proceedings of the IEEE/CVF conference on computer vision and pattern recognition*, pages 15262–15271, 2021. 1, 5
- [17] Geoffrey Hinton. Distilling the knowledge in a neural network. *arXiv preprint arXiv:1503.02531*, 2015. 2
- [18] Geoffrey E Hinton and Sam Roweis. Stochastic neighbor embedding. *Advances in neural information processing systems*, 15, 2002. 3, 4
- [19] Grant Van Horn, Oisín Mac Aodha, Yang Song, Yin Cui, Chen Sun, Alex Shepard, Hartwig Adam, Pietro Perona, and Serge Belongie. The inaturalist species classification and detection dataset, 2018. 5

- [20] Jonathan Krause, Michael Stark, Jia Deng, and Li Fei-Fei. 3d object representations for fine-grained categorization. In *Proceedings of the IEEE international conference on computer vision workshops*, pages 554–561, 2013. 5
- [21] Alex Krizhevsky, Geoffrey Hinton, et al. Learning multiple layers of features from tiny images. 2009. 5, 7
- [22] Ananya Kumar, Aditi Raghunathan, Robbie Jones, Tengyu Ma, and Percy Liang. Fine-tuning can distort pretrained features and underperform out-of-distribution. In *International Conference on Learning Representations*, 2022. 7
- [23] Jae-Hun Lee, Doyoung Yoon, ByeongMoon Ji, Kyungyul Kim, and Sangheum Hwang. Rethinking evaluation protocols of visual representations learned via self-supervised learning. *arXiv preprint arXiv:2304.03456*, 2023. 5
- [24] Zhichao Lu, Gautam Sreeksumar, Erik Goodman, Wolfgang Banzhaf, Kalyanmoy Deb, and Vishnu Naresh Boddeti. Neural architecture transfer. *IEEE transactions on pattern analysis and machine intelligence*, 43(9):2971–2989, 2021. 7, 8
- [25] Avner Magen. Dimensionality reductions in l2 that preserve volumes and distance to affine spaces. *Discrete & Computational Geometry*, 38:139–153, 2007. 2
- [26] Subhransu Maji, Esa Rahtu, Juho Kannala, Matthew Blaschko, and Andrea Vedaldi. Fine-grained visual classification of aircraft. *arXiv preprint arXiv:1306.5151*, 2013. 5
- [27] Anh Nguyen, Jason Yosinski, and Jeff Clune. Deep neural networks are easily fooled: High confidence predictions for unrecognizable images. In *Proceedings of the IEEE conference on computer vision and pattern recognition*, pages 427–436, 2015. 1
- [28] Maria-Elena Nilsback and Andrew Zisserman. Automated flower classification over a large number of classes. In *2008 Sixth Indian conference on computer vision, graphics & image processing*, pages 722–729. IEEE, 2008. 5
- [29] Maxime Oquab, Timothée Darcet, Théo Moutakanni, Huy Vo, Marc Szafraniec, Vasil Khalidov, Pierre Fernandez, Daniel Haziza, Francisco Massa, Alaaeldin El-Nouby, et al. Dinov2: Learning robust visual features without supervision. *arXiv preprint arXiv:2304.07193*, 2023. 1, 2, 3, 4, 5, 6, 7
- [30] Omkar M Parkhi, Andrea Vedaldi, Andrew Zisserman, and CV Jawahar. Cats and dogs. In *2012 IEEE conference on computer vision and pattern recognition*, pages 3498–3505. IEEE, 2012. 5, 7
- [31] Alec Radford, Jong Wook Kim, Chris Hallacy, Aditya Ramesh, Gabriel Goh, Sandhini Agarwal, Girish Sastry, Amanda Askell, Pamela Mishkin, Jack Clark, et al. Learning transferable visual models from natural language supervision. In *International conference on machine learning*, pages 8748–8763. PMLR, 2021. 1, 2
- [32] Benjamin Recht, Rebecca Roelofs, Ludwig Schmidt, and Vaishal Shankar. Do imagenet classifiers generalize to imagenet? In *International conference on machine learning*, pages 5389–5400. PMLR, 2019. 5
- [33] Olga Russakovsky, Jia Deng, Hao Su, Jonathan Krause, Sanjeev Satheesh, Sean Ma, Zhiheng Huang, Andrej Karpathy, Aditya Khosla, Michael Bernstein, Alexander C. Berg, and Li Fei-Fei. ImageNet Large Scale Visual Recognition Challenge. *International Journal of Computer Vision (IJCV)*, 115(3):211–252, 2015. 5
- [34] Mark Sandler, Andrew Howard, Menglong Zhu, Andrey Zhmoginov, and Liang-Chieh Chen. Mobilenetv2: Inverted residuals and linear bottlenecks. In *Proceedings of the IEEE conference on computer vision and pattern recognition*, pages 4510–4520, 2018. 7
- [35] Xiaoxiao Sun, Xingjian Leng, Zijian Wang, Yang Yang, Zi Huang, and Liang Zheng. CIFAR-10-warehouse: Broad and more realistic testbeds in model generalization analysis. In *The Twelfth International Conference on Learning Representations*, 2024. 7, 8
- [36] Yiyu Sun, Yifei Ming, Xiaojin Zhu, and Yixuan Li. Out-of-distribution detection with deep nearest neighbors, 2022. 2
- [37] Hugo Touvron, Matthieu Cord, Matthijs Douze, Francisco Massa, Alexandre Sablayrolles, and Hervé Jégou. Training data-efficient image transformers & distillation through attention. In *International conference on machine learning*, pages 10347–10357. PMLR, 2021. 3, 7, 8
- [38] Laurens Van der Maaten and Geoffrey Hinton. Visualizing data using t-sne. *Journal of machine learning research*, 9(11), 2008. 3, 4
- [39] Sagar Vaze, Kai Han, Andrea Vedaldi, and Andrew Zisserman. Open-set recognition: A good closed-set classifier is all you need. In *International Conference on Learning Representations*, 2022. 5
- [40] Haoan Wang, Songwei Ge, Zachary Lipton, and Eric P Xing. Learning robust global representations by penalizing local predictive power. *Advances in Neural Information Processing Systems*, 32, 2019. 5
- [41] Haoqi Wang, Zhizhong Li, Litong Feng, and Wayne Zhang. Vim: Out-of-distribution with virtual-logit matching. In *Proceedings of the IEEE/CVF Conference on Computer Vision and Pattern Recognition (CVPR)*, pages 4921–4930, 2022. 5
- [42] Longhui Wei, An Xiao, Lingxi Xie, Xiaopeng Zhang, Xin Chen, and Qi Tian. Circumventing outliers of autoaugment with knowledge distillation. In *European Conference on Computer Vision*, pages 608–625. Springer, 2020. 3
- [43] Peter Welinder, Steve Branson, Takeshi Mita, Catherine Wah, Florian Schroff, Serge Belongie, and Pietro Perona. Caltech-ucsd birds 200. 2010. 5
- [44] Zhirong Wu, Yuanjun Xiong, Stella X Yu, and Dahua Lin. Unsupervised feature learning via non-parametric instance discrimination. In *Proceedings of the IEEE conference on computer vision and pattern recognition*, pages 3733–3742, 2018. 5
- [45] Jingkang Yang, Pengyun Wang, Dejian Zou, Zitang Zhou, Kunyuan Ding, Wenxuan Peng, Haoqi Wang, Guangyao Chen, Bo Li, Yiyu Sun, et al. Openood: Benchmarking generalized out-of-distribution detection. *Advances in Neural Information Processing Systems*, 35:32598–32611, 2022. 1, 5, 7, 8, 2, 3, 4
- [46] Zhendong Yang, Zhe Li, Mingqi Shao, Dachuan Shi, Zehuan Yuan, and Chun Yuan. Masked generative distillation. In *European Conference on Computer Vision*, pages 53–69. Springer, 2022. 3

- [47] Zhendong Yang, Zhe Li, Ailing Zeng, Zexian Li, Chun Yuan, and Yu Li. Vitkd: Feature-based knowledge distillation for vision transformers. In *Proceedings of the IEEE/CVF Conference on Computer Vision and Pattern Recognition*, pages 1379–1388, 2024. [3](#)
- [48] Kun Yuan, Shaopeng Guo, Ziwei Liu, Aojun Zhou, Fengwei Yu, and Wei Wu. Incorporating convolution designs into visual transformers. In *Proceedings of the IEEE/CVF international conference on computer vision*, pages 579–588, 2021. [7](#), [8](#)
- [49] Sangdoon Yun, Dongyoon Han, Seong Joon Oh, Sanghyuk Chun, Junsuk Choe, and Youngjoon Yoo. Cutmix: Regularization strategy to train strong classifiers with localizable features, 2019. [8](#), [9](#)
- [50] Hongyi Zhang, Moustapha Cisse, Yann N. Dauphin, and David Lopez-Paz. mixup: Beyond empirical risk minimization, 2018. [8](#)
- [51] Shaoting Zhang and Dimitris Metaxas. On the challenges and perspectives of foundation models for medical image analysis. *Medical image analysis*, 91:102996, 2024. [1](#)
- [52] Yitian Zhang, Xu Ma, Yue Bai, Huan Wang, and Yun Fu. Accessing vision foundation models at imagenet-level costs, 2024. [2](#), [3](#), [4](#), [5](#), [9](#)
- [53] Jinghao Zhou, Chen Wei, Huiyu Wang, Wei Shen, Cihang Xie, Alan Yuille, and Tao Kong. ibot: Image bert pre-training with online tokenizer. *arXiv preprint arXiv:2111.07832*, 2021. [2](#), [3](#)

# Faithful Label-free Knowledge Distillation

## Supplementary Material

### A. The Johnson–Lindenstrauss Lemma

The Johnson–Lindenstrauss (JL) Lemma [13] states that for a set of points  $\mathbf{X}$  in a high dimensional space, there exists a function that can map these points into a lower dimensional space, within error  $\epsilon$ , where this error depends on the dimension of the lower dimensional space  $m$  and the size of the set of points  $|\mathbf{X}|$ . In its standard form, the JL lemma states that Euclidean distances are preserved.

**Lemma A.1** (Johnson–Lindenstrauss) *For every  $d \in \mathbb{N}_1$ ,  $\epsilon \in (0, 1)$  and  $\mathbf{X} \subset \mathbb{R}^d$ , there exists a function  $f : \mathbb{R}^d \rightarrow \mathbb{R}^m$  where  $m = \Theta(\epsilon^{-2} \log |\mathbf{X}|)$  such that for every  $x, y \in \mathbf{X}$ ,*

$$||f(x) - f(y)||_2^2 - ||x - y||_2^2 \leq \epsilon ||x - y||_2^2 \quad (12)$$

Moreover, the map  $f$  can be constructed using a simple approach. Given a matrix  $M \in \mathbb{R}^{m \times d}$  with every element drawn from a standard normal distribution, then

$$f(x) := \frac{1}{\sqrt{m}} Mx \quad (13)$$

is a linear map that satisfies Lemma A.1 with a probability given by the norm preservation lemma.

**Lemma A.2** (Norm preservation) *Let  $\epsilon \in (0, 1)$ . If  $f$  is constructed as above with  $m = \Theta(\epsilon^{-2} \log \delta^{-1})$ , and  $x \in \mathbb{R}^m$  is a unit vector, then*

$$\mathbb{P} [||f(x)||_2^2 \in (1 \pm \epsilon)] \geq 1 - \delta \quad (14)$$

Again, for target spaces with larger dimension  $m$  this Lemma states that it is more likely that a high quality map will be sampled.

A similar result also holds for angles [25], which gives

**Lemma A.3** (Angles) *Let  $\epsilon < \frac{1}{3}$  and let  $n, t$  be integers for which  $t > 60\epsilon^{-2} \log n$ . Then for any  $n$ -point subset  $X$  of the Euclidean space  $\mathbb{R}^N$ , there is a linear contracting embedding  $f(X) \rightarrow \mathbb{R}^t$ , under which angles are preserved to within a (double-sided) factor of  $1 + 8/\pi\sqrt{\epsilon}$ .*

The proof of this statement also relies on  $f$  being generated as a random projection as above [25].

### B. Further Results

**Larger teachers result in better accuracy but have poorer quality dense features.** We observe that training with larger teachers in comparison to the student requires longer training runs. To achieve best results efficiently, the pretrained models from a smaller teacher are used as a starting point. Then, the student and teacher heads are first trained with a frozen pretrained student model (allowing the TinTem teacher heads to minimize the student loss) for 30 epochs. Finally, the models are trained for 300 epochs using the same distillation approach as previously. Tab. S13 shows that this improves the performance of the student models, with TinTeM seeing larger improvements in accuracy on ImageNet-1K in comparison to Proteus.

However, this results in poorer results in dense image tasks, like semantic segmentation. Tab. S14 shows that the students trained with a larger teacher network have poorer mIoU for a linear probe on the Pascal VOC 2012 dataset. Undertaking longer distillation runs, or continuing training using a larger image resolution potentially might be helpful in these cases.

**Further out-of-distribution detection results.** The OOD detection results for all of the OpenOOD datasets [45] are presented in Tab. S15, Tab. S16 and Tab. S17. The tables report the ROC-AUC for detecting OOD images and the False Positive Rate (FPR) using a 95% threshold for including all in-distribution images. To produce these results, the KNN+ [36] OOD metric is used to measure the performance of the model backbones. For ImageNet-1K, we sample 1% of the dataset (12,812 images) and set  $k = 10$  to measure distance to OOD samples. For CIFAR-10/100, we sample 100% of the dataset (50,000 images) and set  $k = 1$ .

Table S13. **ImageNet classification — larger teachers.** Comparison of performance on ImageNet-1K under kNN and linear probing evaluation approaches.

Method	Arch	Teacher	kNN				Linear
			Backbone	Student head	Teacher head	Teacher	
Proteus	ViT-Ti/14	DINOv2 ViT-S/14	73.1	73.5		79.0	76.1
TinTeM	ViT-Ti/14	DINOv2 ViT-S/14	<b>74.3</b>		78.8	79.0	<b>76.8</b>
Proteus	ViT-Ti/14	DINOv2 ViT-B/14	73.4	73.8		82.1	76.9
TinTeM	ViT-Ti/14	DINOv2 ViT-B/14	<b>75.6</b>		81.9	82.1	<b>77.9</b>

Table S14. **Semantic segmentation — larger teachers.** Comparison of performance on the Pascal VOC 2012 semantic segmentation task using a linear probe.

Method	Arch	Teacher	mIoU
Proteus	ViT-Ti/14	DINOv2 ViT-S/14	70.5
TinTeM	ViT-Ti/14	DINOv2 ViT-S/14	<b>71.1</b>
Proteus	ViT-Ti/14	DINOv2 ViT-B/14	68.1
TinTeM	ViT-Ti/14	DINOv2 ViT-B/14	<b>69.7</b>

Table S15. **Out-of-distribution detection.** Comparison of performance on the OpenOOD benchmark for the ImageNet-1K dataset. The  $\uparrow$  means larger values are better and the  $\downarrow$  means smaller values are better.

Method	Arch	Teacher	Near OOD Datasets						Far OOD Datasets							
			SSB-hard		NINCO		Average		iNaturalist		OpenImage-O		Textures		Average	
			AUROC $\uparrow$	FPR $\downarrow$	AUROC $\uparrow$	FPR $\downarrow$	AUROC $\uparrow$	FPR $\downarrow$	AUROC $\uparrow$	FPR $\downarrow$	AUROC $\uparrow$	FPR $\downarrow$	AUROC $\uparrow$	FPR $\downarrow$	AUROC $\uparrow$	FPR $\downarrow$
Proteus	ViT-Ti/14	DINOv2 ViT-S/14	55.59	92.24	72.76	79.22	64.17	85.73	60.08	91.47	73.13	75.34	<b>89.46</b>	<b>37.1</b>	74.22	67.97
TinTeM	ViT-Ti/14	DINOv2 ViT-S/14	<b>63.39</b>	<b>84.98</b>	<b>77.58</b>	<b>69.59</b>	<b>70.49</b>	<b>77.29</b>	<b>95.81</b>	<b>22.57</b>	<b>90.72</b>	<b>40.62</b>	86.57	48.45	<b>91.03</b>	<b>37.21</b>
		DINOv2 ViT-S/14	65.76	81.8	79.39	66.45	72.58	74.12	98.74	4.76	92.23	35.44	87.04	48.45	92.67	29.55
Proteus	ViT-S/14	DINOv2 ViT-B/14	53.78	97.4	68.61	91.71	61.19	94.56	39.89	99.5	61.7	91.11	84.19	69.73	61.92	86.78
TinTeM	ViT-S/14	DINOv2 ViT-B/14	<b>65.75</b>	<b>82.98</b>	<b>81.24</b>	<b>64.71</b>	<b>73.5</b>	<b>73.84</b>	<b>97.31</b>	<b>12.27</b>	<b>92.77</b>	<b>32.95</b>	<b>88.72</b>	<b>41.71</b>	<b>92.93</b>	<b>28.98</b>

Table S16. **Specialist models — near OOD detection.** Comparison of performance on the OpenOOD benchmark [45]. The  $\uparrow$  means larger values are better and the  $\downarrow$  means smaller values are better.

IDD	Method	Arch	Teacher	Pretraining dataset	Near OOD Datasets						Average	
					CIFAR-10		CIFAR-100		Tiny ImageNet		Average	
					AUROC $\uparrow$	FPR $\downarrow$	AUROC $\uparrow$	FPR $\downarrow$	AUROC $\uparrow$	FPR $\downarrow$	AUROC $\uparrow$	FPR $\downarrow$
<b>CIFAR-100</b>												
Frozen	DeiT	ViT-Ti/16	RegNetY-16GF	ImageNet	53.53	94.96			62.75	85.44	58.14	90.2
	TinTeM	ViT-Ti/14	DINOv2 ViT-S/14	ImageNet	80.39	71.45			90.07	34.94	85.23	53.2
	TinTeM	ViT-Ti/14	DINOv2 ViT-S/14	ImageNet $\rightarrow$ Target dataset	84.08	70.28			89.91	44.15	87.0	57.22
DeiT finetuned	DeiT	ViT-Ti/16	RegNetY-16GF	ImageNet	83.91	61.04			90.98	44.29	87.45	52.66
	TinTeM	ViT-Ti/14	DINOv2 ViT-S/14	ImageNet	85.45	56.76			90.34	47.36	87.9	52.06
	TinTeM	ViT-Ti/14	DINOv2 ViT-S/14	ImageNet $\rightarrow$ Target dataset	86.7	56.45			92.35	39.37	89.52	47.91
<b>CIFAR-10</b>			DINOv2 ViT-S/14		87.97	56.05			91.83	29.61	89.9	42.83
Frozen	DeiT	ViT-Ti/16	RegNetY-16GF	ImageNet			50.88	94.08	63.15	84.75	57.01	89.42
	TinTeM	ViT-Ti/14	DINOv2 ViT-S/14	ImageNet			90.22	41.5	96.67	13.63	93.44	27.57
	TinTeM	ViT-Ti/14	DINOv2 ViT-S/14	ImageNet $\rightarrow$ Target dataset			93.76	31.79	96.49	15.86	95.12	23.82
DeiT finetuned	DeiT	ViT-Ti/16	RegNetY-16GF	ImageNet			96.5	16.34	97.08	12.52	96.79	14.43
	TinTeM	ViT-Ti/14	DINOv2 ViT-S/14	ImageNet			96.15	16.57	97.24	10.62	96.69	13.6
	TinTeM	ViT-Ti/14	DINOv2 ViT-S/14	ImageNet $\rightarrow$ Target dataset			96.76	15.94	97.33	12.02	97.05	13.98
			DINOv2 ViT-S/14				94.08	29.27	97.59	10.28	95.83	19.77

Table S17. **Specialist models — far OOD detection.** Comparison of performance on the OpenOOD benchmark [45]. The  $\uparrow$  means larger values are better and the  $\downarrow$  means smaller values are better.

IDD	Method	Arch	Teacher	Pretraining dataset	Far OOD Datasets								Average	
					DTD		MNIST		SVHN		Places365		AUROC $\uparrow$	FPR $\downarrow$
					AUROC $\uparrow$	FPR $\downarrow$	AUROC $\uparrow$	FPR $\downarrow$	AUROC $\uparrow$	FPR $\downarrow$	AUROC $\uparrow$	FPR $\downarrow$		
<b>CIFAR-100</b>														
Frozen	DeiT	ViT-Ti/16	RegNetY-16GF	ImageNet	14.97	100.0	71.86	73.77	43.35	93.18	54.57	83.06	46.19	87.5
	TinTeM	ViT-Ti/14	DINOv2 ViT-S/14	ImageNet	33.09	99.89	97.21	11.01	76.96	87.71	98.22	7.18	76.37	51.45
	TinTeM	ViT-Ti/14	DINOv2 ViT-S/14	ImageNet $\rightarrow$ Target dataset	44.46	98.56	95.78	18.94	86.17	67.34	97.39	12.91	80.95	49.44
DeiT finetuned	DeiT	ViT-Ti/16	RegNetY-16GF	ImageNet	74.07	82.86	85.18	62.99	95.81	24.57	91.87	43.29	86.73	53.43
	TinTeM	ViT-Ti/14	DINOv2 ViT-S/14	ImageNet	83.41	68.51	87.49	56.64	96.5	21.0	92.08	37.52	89.87	45.92
	TinTeM	ViT-Ti/14	DINOv2 ViT-S/14	ImageNet $\rightarrow$ Target dataset	79.51	67.44	90.24	48.05	96.12	22.84	92.27	37.61	89.53	43.98
<b>CIFAR-10</b>														
					42.46	99.8	96.25	15.68	77.75	88.13	97.89	8.48	78.58	53.02
Frozen	DeiT	ViT-Ti/16	RegNetY-16GF	ImageNet	17.03	100.0	71.36	73.15	42.03	92.25	57.74	80.58	47.04	86.49
	TinTeM	ViT-Ti/14	DINOv2 ViT-S/14	ImageNet	95.24	30.79	99.17	3.54	89.13	60.24	99.97	0.18	95.87	23.69
	TinTeM	ViT-Ti/14	DINOv2 ViT-S/14	ImageNet $\rightarrow$ Target dataset	98.2	7.44	98.92	4.38	95.08	33.79	99.88	0.48	98.02	11.52
DeiT finetuned	DeiT	ViT-Ti/16	RegNetY-16GF	ImageNet	97.86	9.33	97.52	9.69	99.67	0.71	99.7	0.96	98.69	5.17
	TinTeM	ViT-Ti/14	DINOv2 ViT-S/14	ImageNet	97.95	9.31	97.41	8.99	99.63	0.32	99.36	1.51	98.59	5.03
	TinTeM	ViT-Ti/14	DINOv2 ViT-S/14	ImageNet $\rightarrow$ Target dataset	97.78	11.81	98.18	7.9	99.81	0.16	99.37	2.16	98.79	5.51
					97.0	19.08	98.93	4.25	90.6	55.45	99.96	0.18	96.62	19.74

Table S18. **Ablation study: weighting.** Comparison of kNN performance on ImageNet-1K for TinTeM models trained with different weightings  $\gamma$  for the dimensionality reduction component. The first row uses the frozen gradient approach described in the paper.

Method	Arch	Teacher	$\gamma$	kNN
TinTeM	ViT-Ti/14	DINOv2 ViT-S/14	-	74.3
TinTeM	ViT-Ti/14	DINOv2 ViT-S/14	10	74.3
TinTeM	ViT-Ti/14	DINOv2 ViT-S/14	100	74.2

Table S19. **Ablation study: metric.** Comparison of kNN performance on ImageNet-1K for TinTeM models trained with different metrics for the student loss.

Method	Arch	Teacher	Loss Metric	kNN
TinTeM	ViT-Ti/14	DINOv2 ViT-S/14	<b>Cosine distance</b>	74.3
TinTeM	ViT-Ti/14	DINOv2 ViT-S/14	MSE	74.2

## C. Ablation studies

In this section we modify a number of hyperparameters and component choices for TinTeM to investigate how these impact performance. In the tables below the bold parameter sets are the default ones used throughout the rest of the paper.

**TinTeM dimensionality reduction loss weighting.** We consider the performance of weighting the dimensionality reduction loss in Eq. (2), rather than freezing the gradients of  $\phi$  in the student loss. This gives an alternative loss function

$$\mathcal{L}_{\text{TinTeM}}(\mathbf{X}; \phi, \theta) = \gamma \mathcal{L}_{\text{dim-red}}(\mathbf{X}; \phi) + \mathcal{L}_{\text{student}}(\mathbf{X}; \theta, \phi) \quad (15)$$

where  $\gamma$  is a weighting factor prioritises the dimensionality reduction loss when it is set to be greater than one. Tab. S18 shows that the approach of weighting or freezing gradients leads to similar results.

**TinTeM student loss metric.** Tab. S19 considers the impact on performance of using different metrics for the student loss  $\mathcal{L}_{\text{student}}$  for Eq. (9). It is found that using a cosine distance loss leads to slightly better performance in comparison to a mean squared error loss.

**TinTeM dimensionality reduction temperature parameters.** Tab. S19 shows the performance impact of different sets of temperatures  $\tau$  in the dimensionality reduction loss for Eq. (7). It is found that these values have a small impact on performance, with the best set being  $\tau = [0.10]$ , which obtains slightly better performance than the set of parameters chosen for the paper.

Table S20. **Ablation study: temperature.** Comparison of kNN performance on ImageNet-1K for TinTeM models trained with different sets of temperatures  $\tau$  for the dimensionality reduction loss.

<b>Method</b>	<b>Arch</b>	<b>Teacher</b>	$\tau$	<b>kNN</b>
TinTeM	ViT-Ti/14	DINOv2 ViT-S/14	[0.01, 0.02, 0.03, 0.04, 0.05, 0.06, 0.07, 0.08, 0.09, 0.10]	74.3
TinTeM	ViT-Ti/14	DINOv2 ViT-S/14	[0.01]	74.1
TinTeM	ViT-Ti/14	DINOv2 ViT-S/14	[0.10]	74.5
TinTeM	ViT-Ti/14	DINOv2 ViT-S/14	[0.01, 0.10]	74.3